Geol. Mag. **141** (*4*), *2004, pp. 455–469.* © *2004 Cambridge University Press*
DOI: 10.1017/S0016756804009215 *Printed in the United Kingdom*

Evolution of boninites and island-arc tholeiites in the Pindos Ophiolite, Greece

GEORGIA PE-PIPER*, BASILIOS TSIKOURAS† & KONSTANTIN HATZIPANAGIOTOU†

*Department of Geology, Saint Mary's University, Halifax, Nova Scotia, Canada
†Department of Geology, Section of Earth Materials, University of Patras, Patras, Greece

(*Received* 28 April 2003; *accepted* 27 January 2004)

Abstract – Whole-rock geochemical and Sm/Nd isotope data are presented for a representative suite of crustal rocks from the Pindos Ophiolite in order to resolve the origin of the geochemical signature of the boninites. Comparison is made with Triassic MORB from the Avdella mélange and with other ophiolitic rocks of northwestern Greece. Hydrothermal alteration results in large scatter in Sr and K and some variability in Ba, Th and U. The Pindos boninites contain high Zr and Hf with respect to REE, characteristic of many boninites. Pb, La/Sm and Nb decrease with decreasing TiO_2 from MORB to IAT, but then increase in the boninites. Nd isotopic values expressed as ε_{Nd} decrease systematically with decreasing TiO_2, from 7–8 in IAT to 0.6–3.0 in boninites. As mantle wedge harzburgite became increasingly depleted, another magma source contributed significant amounts of Pb, REE and probably Nb. The Pb and other large-ion lithophile elements may have been transported in aqueous solutions from the subducting slab, but the REE and Nb imply an ocean-island basalt (OIB)-type source within the mantle wedge. This OIB source is a consequence of mantle plume activity during late Triassic rifting.

Keywords: Nd isotopes, basalt, Jurassic, geochemistry, ocean-island basalt.

1. Introduction

Many ophiolite complexes include late magmatic dykes, highly depleted in high-field strength elements, that are known as boninites. The Jurassic Pindos Ophiolite of western Greece is a classical example of a supra-subduction ophiolite (Pearce, Lippard & Roberts, 1984) which shows a wide range of magma types represented by lavas and cross-cutting dykes, the details of which were resolved by Kostopoulos (D. Kostopoulos, unpub. Ph.D. thesis, Univ. Newcastle, 1989) and Jones, Robertson & Cann (1991). The rocks range from high-Ti mid-ocean ridge basalt (MORB) through island-arc tholeiites (IAT) to boninites, and cross-cutting relationships show that the more evolved IAT and boninites are progressively younger. These rocks were emplaced in a supra-subduction ophiolitic setting, meaning that the same mantle wedge sourced all the magmas. This mantle wedge was progressively depleted through time as a result of melt extraction and modified by fluids and possibly silicic magmas from the subducting slab or deeper mantle. These changes are reflected by the change through time from MORB to IAT to boninite rocks. Changes in Nd isotopic composition and trace element composition reflect sourcing of these elements from elsewhere than the main depleted harzburgite of the mantle wedge.

* Author for correspondence: gpiper@smu.ca

In this paper, we try to evaluate the origin of boninite magmas of the Pindos Ophiolite on the basis of Nd isotope and trace element compositions with the aim to identify the provenance of these elements as the harzburgite source became increasingly refractory. Studies of boninites elsewhere indicate that the most likely sources of such elements are either from the subducting slab, including subducted terrigenous sediments (e.g. Rogers, MacLeod & Murton, 1989; Taylor *et al*. 1994), or from the influence of ocean island basalt (OIB)-type melt (e.g. Kostopoulos & Murton, 1992; Wendt *et al*. 1997). Because much of the classic work on the Pindos Ophiolite (Capedri *et al*. 1980, 1981; Capedri, Venturelli & Toscani, 1982; Dupuy *et al*. 1984) was carried out decades ago, new rock chemical analyses were necessary to make such an assessment for the Pindos Ophiolite.

2. Geological and petrological framework

The Pindos Ophiolite Complex, together with the Vourinos Complex, are the best known ophiolite complexes of Greece and are thought to be continuous beneath the Oligocene–Miocene post-orogenic basin of the Mesohellenic Trough (Jones, Robertson & Cann, 1991; Rassios & Smith, 2000). They were emplaced from the Pindos ocean onto the Pelagonian continental margin in the late Jurassic (likely in the Kimmeridgian). The Pindos Ophiolite (Fig. 1) consists of three main thrust sheets: the Dramala Complex, the Loumnitsa

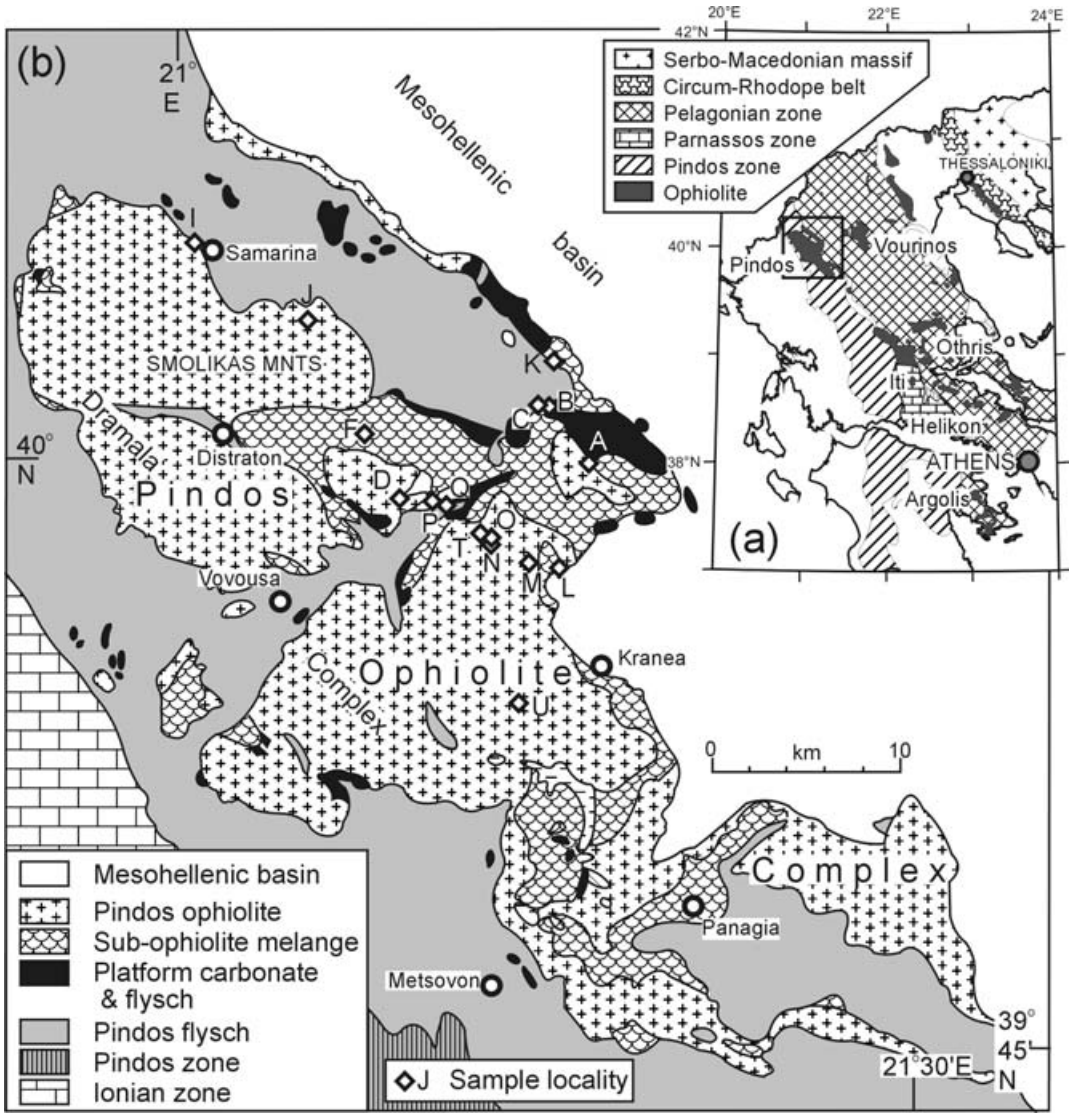

Figure 1. (a) Relationship of Pindos Ophiolite Complex to other ophiolites of western Greece. (b) Geological map of the Pindos Ophiolite Complex (modified from Jones & Robertson, 1991), showing location of samples.

Unit and the Aspropotamos Complex, all structurally overlying the Avdella mélange (Jones & Robertson, 1991).

The Dramala Complex consists of harzburgite peridotite with abundant podiform dunite and some plagioclase lherzolite. Pyroxenite dykes and rodingitized gabbro dykelets cut the peridotite (Capedri, Garuti & Rossi, 1978). The harzburgite is overlain by crustal cumulates, including plagioclase-dunite–troctolite–anorthosite gabbro (leucogabbro) cumulates interlayered with wehrlites (Capedri, Venturelli & Toscani, 1982; Rassios, 1991).

The reconstructed stratigraphy of eastern Aspropotamos Complex (D. Kostopoulos, unpub. Ph.D. thesis, Univ. Newcastle, 1989) is a basal series of mafic and ultramafic cumulates overlain by gabbro and minor plagiogranites and sheeted dykes capped by a series of extrusives. The sheeted dykes are of various types, from oldest to youngest of high-Ti MORB, IAT and boninitic composition. The extrusive lavas show the same range of geochemical types. The western Aspropotamos Complex is more dismembered than the eastern part of the complex. In the western complex, the basal isotropic gabbros are olivine bearing and pass up into quartz-bearing gabbros with plagiogranite pods. These are overlain by sheeted dykes and then by lavas, principally of bonititic composition, but including some IAT/boninite lavas (D. Kostopoulos, unpub. Ph.D. thesis, Univ. Newcastle, 1989). Overall, the following chronological sequence of dykes was inferred by Kostopoulos: high-Ti MORB (Moura dykes), transitional MORB/IAT (Gortsia dykes), IAT (Padia Verdi dykes), transitional IAT/boninite (‘dolerite’ dykes) and boninite (N50E dykes).

The Loumnitsa Unit is the basal metamorphic sole of both the Dramala and Aspropotamos complexes,

https://doi.org/10.1017/S0016756804009215 Published online by Cambridge University Press

comprising lower amphibolite and greenschist-facies meta-igneous and metasedimentary rocks that have yielded Ar–Ar ages of 169 ± 5 and 165 ± 3 Ma (Whitechurch & Parrot, 1978; Spray & Roddick, 1980). The Avdella mélange is about 1 km thick and comprises blocks in matrix and mappable thrust sheets (Jones & Robertson, 1991). Various rock types are present, which in approximate order of abundance are: ophiolite-derived volcaniclastic turbidites, radiolarites, quartzo-feldspathic turbidite sandstones and shales, pelagic limestones, serpentinite and both alkaline and MORB basalt.

3. Sampling and analytical methods

To solve the problem we posed in the introduction of this paper we tried to obtain a complete sample set of the Pindos magmas: MORB, transitional MORB/IAT, IAT and boninite. In the field, the freshest available samples were collected. Thus, a set of thirty-five analytical samples was finally selected, based on their location and petrography (see Appendix), that represents all magmatic rock types that have been discussed in the literature for the Pindos Ophiolite.

All thirty-five samples were analysed for major and trace elements by X-ray fluorescence (XRF) using fused beads for major elements and pressed pellets for trace elements (Tables 1, 2). Particular attention was paid to determinations of Nb and Zr. In addition, we analysed five samples of probable Triassic volcanic rocks from the Avdella mélange (Table 3). Accuracy for SiO_2 is within 0.5%, $< 1\%$ for other major elements and $< 5\%$ for trace elements. Instrumental precision is $< 0.6\%$ relative and sample precision $< 0.7\%$ relative for trace elements and $< 1\%$ for major elements. Detection limits are 1 ppm for Nb, 3 ppm for Ni, Y and Pb, 4 ppm for Cr, Zr and V, and 0.005% for Ti.

Eleven representative samples were analysed for rare earth elements (REE) and selected trace elements including Th, U and Hf by instrumental neutron activation analysis (INAA). Detection limit is 0.01 ppm for Sm and Lu, 0.05 ppm for La, Eu and Yb, 0.1 ppm for Tb, U and Th, 0.2 ppm for Hf, and 1 ppm for Ce and Nd. Seven samples have been analysed for Sm/Nd isotopes (Table 4) (method and errors as in Pe-Piper & Piper, 2002, appendix 2). The loss on ignition (LOI) for all samples analysed for REE and Sm/Nd isotopes was $< 3.1\%$. Sm/Nd isotopic data are displayed as ε_{Nd} values relative to the chondritic uniform reservoir (CHUR) at the age of crystallization, assumed to be 165 Ma (Table 4). This age is based on $^{40}Ar/^{39}Ar$ radiometric ages from soles of the Pindos and correlative ophiolites, which range from 171 to 165 Ma (Spray & Roddick, 1980), and the occurrence of radiolarites with ophiolitic detritus, which date from Bathonian–Callovian times (159–169 Ma) (Robertson *et al*. 1991).

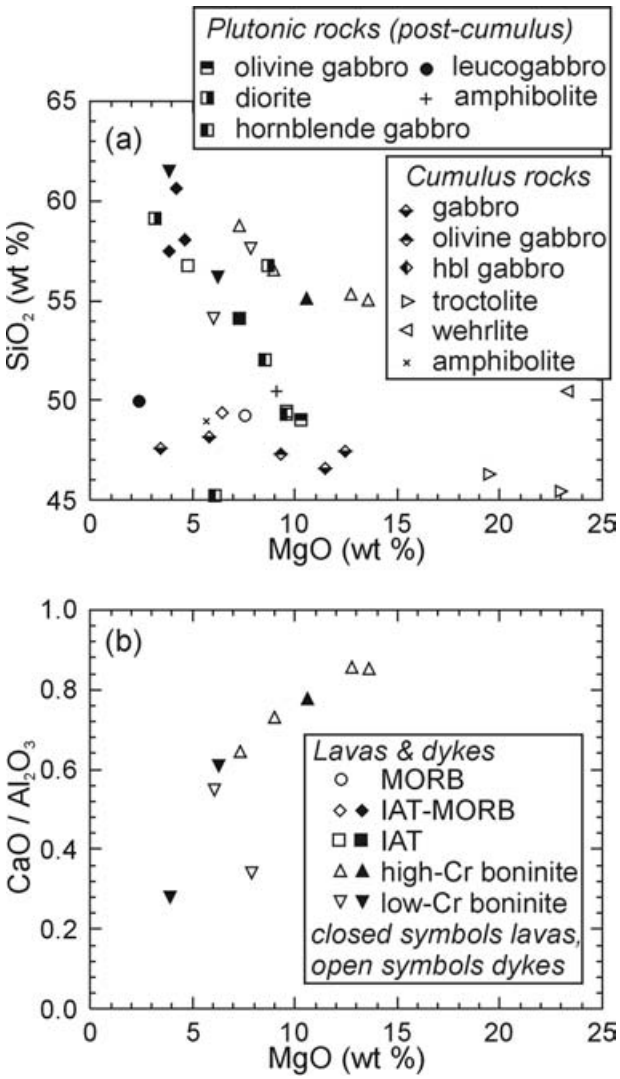

Figure 2. (a) Variation of SiO_2 with MgO for all the analysed samples from the Pindos Ophiolite Complex; (b) variation of CaO/Al_2O_3 with MgO for boninite samples only.

4. Geochemical signatures

4.a. Identification of geochemical type

The major element variation shows the presence of lavas and dykes with SiO_2 contents ranging from 49% to 62 wt% (volatile free) (Fig. 2a). High MgO contents (all but one 6–16% MgO) of lavas and dykes with 54–62% SiO_2 are characteristic of boninites. The SiO_2 v. MgO (Fig. 2a) and CaO/Al_2O_3 v. MgO (Fig. 2b) composition are both characteristic of high-Ca boninites (Falloon & Crawford, 1991). Post-cumulus gabbro and diorite show a range of SiO_2 v. MgO compositions similar to the lavas (Fig. 2a).

Our nomenclature is based on variation in the immobile elements Ti and Zr (Figs 3, 4), by comparison with nomenclature used by other authors who have studied Greek ophiolites (e.g. Dupuy *et al*. 1984; Jones, Robertson & Cann, 1991; Capedri *et al*. 1980; Capedri *et al*. 1996; Dostal *et al*. 1991). Chemical analyses of

https://doi.org/10.1017/S0016756804009215 Published online by Cambridge University Press

Table 1. Whole rock chemical analyses of lavas and dykes from the Pindos Ophiolite

Sample	P2	P3	P6	P12i	P13	P14i	P15	P22ii	P39	P42	P45	P53i	P58	P59	P61i	P63	P64
Chemical affinity	Low-Cr boninite	Low-Cr boninite	High-Cr boninite	Low-Cr boninite	IAT	IAT/ MORB	IAT	High-Cr boninite	IAT/ MORB	IAT/ MORB	IAT/ MORB	High-Cr boninite	High-Cr boninite	High-Ti MORB	IAT	High-Cr boninite	Low-Cr boninite
Rock type	Dyke	Lava	Lava	Lava	Dyke	Lava	Lava	Dyke	Lava	Lava	Dyke	Dyke	Dyke	Dyke	Dyke	Dyke	Dyke
Locality	A	A	A	B	B	B	C	F	K	M	N	R	U	U	U	U	U
Major elements by XRF (wt %)																	
SiO_2	54.69	54.87	54.04	57.92	54.91	53.91	52.97	55.31	56.45	58.55	48.97	53.97	58.12	48.41	49.34	53.68	52.77
TiO_2	0.34	0.21	0.24	0.27	0.60	0.87	0.69	0.21	1.07	0.89	0.86	0.19	0.20	1.87	0.73	0.17	0.30
Al_2O_3	14.39	15.03	12.82	13.91	14.71	14.24	15.76	12.80	14.79	14.60	18.32	11.10	14.14	14.02	15.62	10.96	15.25
Fe_2O_{3T}	9.46	9.49	9.21	9.00	10.49	10.16	10.07	9.77	11.41	8.72	8.43	8.89	8.53	12.61	9.34	9.18	9.72
MnO	0.13	0.15	0.16	0.10	0.16	0.13	0.21	0.16	0.28	0.10	0.13	0.14	0.14	0.18	0.13	0.16	0.16
MgO	7.45	6.11	10.43	3.68	4.64	3.65	7.18	8.80	4.51	4.09	6.46	13.32	7.24	7.45	9.59	12.36	5.93
CaO	4.88	9.14	9.98	3.88	7.33	4.93	7.69	9.37	3.27	4.90	13.32	9.48	9.10	10.44	12.53	9.37	8.38
Na_2O	3.37	2.41	1.08	5.34	3.76	5.78	2.80	1.24	5.21	3.94	2.42	0.88	1.29	3.06	2.41	0.90	4.98
K_2O	0.16	0.21	0.11	0.02	0.09	0.03	0.45	0.18	0.11	0.71	0.19	0.05	0.07	0.08	0.11	0.18	0.04
P_2O_5	0.03	0.02	0.03	0.03	0.05	0.07	0.05	0.02	0.09	0.12	0.06	0.02	0.02	0.20	0.04	0.02	0.03
L.O.I	3.90	3.09	3.14	5.19	4.10	5.51	2.82	2.15	3.92	2.91	0.99	2.61	2.00	2.92	1.43	3.13	1.24
Total	98.80	100.73	101.24	99.34	100.84	99.28	100.69	100.01	101.11	99.53	100.15	100.65	100.85	101.24	101.27	100.11	98.80
Trace elements by XRF (ppm)																	
Ba	68	55	b.d.	175	132	5	177	115	b.d.	117	93	b.d.	b.d.	137	82	b.d.	120
Rb	18	17	16	20	15	17	17	16	16	22	16	16	17	11	13	16	16
Sr	57	99	40	14	23	40	83	158	61	120	202	27	43	172	59	25	13
Y	12	13	13	8	20	20	20	14	25	24	30	11	11	40	24	12	15
Zr	24	21	19	22	34	41	35	24	56	68	64	17	20	112	33	16	20
Nb	1.3	2.8	1.4	2.1	1.0	1.1	b.d.	1.6	4.1	2.4	2.5	b.d.	b.d.	5.0	0.4	0.4	0.5
Th	1	2	1	2	b.d.	1	b.d.	b.d.	b.d.	1	2	2	1	b.d.	b.d.	1	1
Pb	6	13	3	8	7	1	b.d.	10	2	b.d.	10	12	6	1	6	7	10
Ga	10	16	9	13	15	15	11	11	17	19	16	10	10	19	18	9	12
Zn	98	74	72	73	74	83	75	76	177	87	78	58	54	97	51	74	76
Cu	289	95	50	119	45	35	85	119	136	57	71	120	592	95	108	121	167
Ni	52	61	140	27	14	11	26	214	15	5	65	269	114	120	146	237	49
V	197	209	188	209	206	249	240	204	259	209	230	182	151	313	202	193	218
Cr	128	92	652	29	25	14	59	525	17	4	233	1035	401	271	473	954	118
Trace elements by INAA (ppm) (where other elements are n.d., La, Ce, Nd, Co, Sc, and U by XRF)																	
La	12	0.62	0.77	10	2	n.d.	1.16	2	15	2.67	3	0.74	0.92	4.46	0.67	0.58	0.95
Ce	51	2	2	16	n.d.	15	3	45	37	9	46	2	2	15	3	2	2
Nd	13	1	1	n.d.	23	19	3	2	33	7	10	1	1	12	3	1	1
Sm	n.d.	0.28	0.34	n.d.	n.d.	n.d.	1.22	n.d.	n.d.	2.35	n.d.	0.31	0.32	4.17	1.38	0.23	0.5
Eu	n.d.	0.12	0.13	n.d.	n.d.	n.d.	0.48	n.d.	n.d.	0.84	n.d.	0.13	0.12	1.45	0.49	n.d.	0.16
Tb	n.d.	0.1	0.1	n.d.	n.d.	n.d.	0.4	n.d.	n.d.	0.6	n.d.	0.1	0.1	0.9	0.4	0.1	0.2
Yb	n.d.	0.91	0.91	n.d.	n.d.	n.d.	1.69	n.d.	n.d.	3.18	n.d.	0.93	1.04	4.37	1.99	0.87	1.3
Lu	n.d.	0.15	0.15	n.d.	n.d.	n.d.	0.27	n.d.	n.d.	0.46	n.d.	0.14	0.16	0.65	0.3	0.14	0.21
Co	44	36.3	43.9	41	44	43	33.3	49	44	23.1	34	51.2	37.6	49.8	47.4	50.2	36
Hf	n.d.	0.4	n.d.	n.d.	n.d.	n.d.	0.8	n.d.	n.d.	1.9	n.d.	n.d.	0.3	3.2	0.9	0.3	0.5
Sc	53	45.3	42.1	36	23	17	35	30	34	28.7	9	45.8	37.2	37.2	36.9	47.7	44.9
Th	n.d.	1	0.2	n.d.	n.d.	n.d.	0.1	n.d.	n.d.	0.2	n.d.	0.2	0.3	0.2	n.d.	n.d.	0.3
U	1	n.d.	n.d.	1	2	1	n.d.	1	1	0.2	1	n.d.	0.2	0.3	n.d.	n.d.	n.d.
ε_{Nd}	n.d.	1.04	1.45	n.d.	n.d.	n.d.	7.04	n.d.	n.d.	n.d.	n.d.	n.d.	n.d.	n.d.	7.61	0.67	3.11

b.d. = below detection limit; n.d. = not determined.

Table 2. Whole rock chemical analyses of plutonic and cumulus rocks from the Pindos Ophiolite

Sample	P4	P5	P9	P10	P11ii	P21	P22i	P31	P32	P37	P46	P49	P50	P51	P52i	P54i	P56	P61ii
Chemical affinity	Cumulus	Low-Cr boninite	IAT	Low-Cr boninite	Cumulus	Cumulus	High-Cr boninite	Cumulus	Cumulus	IAT	IAT/MORB	Cumulus	Cumulus	Cumulus	Cumulus	MORB	Cumulus	IAT/MORB
Rock type	Gabbro	Hbl-gabbro	Leuco-gabbro	Hbl-gabbro	Gabbro	Amphibolite	Diorite	Troctolite	Troctolite	Olivine gabbro	Diorite	Wehrlite	Wehrlite	Gabbro	Olivine gabbro	Amphibolite	Gabbro (altered)	Hbl-gabbro
Locality	A	A	A	A	A	E	F	I	I	J	O	P	P	P	Q	S	T	U
Major elements by XRF (wt %)																		
SiO_2	47.64	44.05	49.11	51.39	46.00	47.97	55.85	45.57	44.29	47.07	56.44	50.01	47.42	46.06	47.03	50.30	46.58	49.71
TiO_2	0.18	1.11	0.45	0.43	0.43	1.22	0.21	0.09	0.08	0.82	1.08	0.09	0.07	0.07	0.12	0.23	0.18	0.78
Al_2O_3	22.67	17.89	25.57	16.04	24.78	14.41	13.01	16.49	14.21	15.48	13.82	1.68	1.25	20.03	22.38	18.86	18.02	15.81
Fe_2O_{3T}	4.50	15.23	5.52	9.06	5.25	10.73	9.66	5.84	6.78	5.56	10.95	7.73	8.39	6.38	3.91	5.01	4.96	9.46
MnO	0.09	0.16	0.07	0.15	0.08	0.16	0.16	0.08	0.10	0.08	0.18	0.15	0.15	0.11	0.06	0.10	0.09	0.16
MgO	5.76	6.00	2.36	8.49	3.37	5.63	8.59	19.24	22.44	9.93	3.03	23.11	25.36	11.40	9.30	9.14	12.25	9.69
CaO	16.31	9.48	11.01	9.36	14.18	14.34	9.64	9.02	7.61	15.69	4.24	16.21	13.69	14.30	15.40	12.35	15.18	13.06
Na_2O	1.63	3.14	3.75	3.56	2.41	3.02	1.14	2.11	1.88	1.36	5.52	0.06	0.05	0.40	1.19	2.93	0.93	2.00
K_2O	0.09	0.27	0.45	0.24	0.10	0.35	0.18	0.02	0.02	0.05	0.04	0.02	0.01	0.03	0.02	0.82	0.02	0.04
P_2O_5	0.01	0.03	0.03	0.03	0.02	0.12	0.02	0.01	0.01	0.02	0.14	0.01	0.01	0.01	0.01	0.01	0.01	0.05
L.O.I	1.61	3.13	2.78	2.51	2.20	1.31	1.94	2.42	3.04	2.71	4.13	1.19	4.28	2.57	0.93	1.67	3.38	0.27
Total	100.49	100.49	101.10	101.26	98.82	99.26	100.40	100.89	100.46	98.77	99.57	100.26	100.68	101.36	100.35	101.42	101.60	101.03
Trace elements by XRF (ppm)																		
Ba	b.d.	21	47	89	b.d.	132	b.d.	149	352	90	b.d.	156	221	b.d.	b.d.	117	b.d.	80
Rb	20	10	23	17	20	11	17	22	21	17	15	14	15	18	20	31	19	13
Sr	133	121	219	97	183	158	161	198	124	196	44	b.d.	b.d.	46	62	308	39	66
Y	6	22	5	14	8	31	14	1	2	23	24	12	10	6	4	7	7	25
Zr	17	21	35	26	26	66	24	22	18	39	45	9	8	12	14	34	13	37
Nb	b.d.	2	1	b.d.	1	2	b.d.	b.d.	b.d.	3	1	b.d.	b.d.	b.d.	b.d.	b.d.	b.d.	1
Th	1	b.d.	2	1	2	b.d.	b.d.	3	3	1	b.d.	b.d.	b.d.	1	3	3	1	b.d.
Pb	7	b.d.	3	2	b.d.	6	3	b.d.	10	1	1	5	3	5	12	1	7	4
Ga	14	18	19	10	20	18	10	8	3	11	18	3	b.d.	11	14	13	7	12
Zn	35	67	31	53	32	87	72	37	41	29	42	43	42	40	27	31	35	57
Cu	44	144	234	31	99	82	110	65	79	6	7	6	26	12	82	28	74	93
Ni	36	66	28	54	30	101	150	912	1091	198	b.d.	473	450	102	258	182	260	140
V	115	872	230	215	173	235	199	30	30	211	184	147	109	74	62	114	85	222
Cr	133	43	11	266	64	307	505	902	1038	428	6	2381	1554	198	828	723	921	450
Trace elements by INAA (ppm) (where other elements are n.d., La, Ce, Nd, Co, Sc, and U by XRF)																		
La	6	0.56	12	n.d.	n.d.	15	n.d.	4	12	2	n.d.	6	14	n.d.	6	5	n.d.	n.d.
Ce	47	2	n.d.	n.d.	n.d.	7	n.d.	n.d.	n.d.	n.d.	11	n.d.	n.d.	n.d.	7	n.d.	n.d.	n.d.
Nd	n.d.	2	n.d.	n.d.	3	15	12	9	2	8	6	20	n.d.	12	2	15	6	19
Sm	n.d.	0.54	n.d.	n.d.	n.d.	n.d.	n.d.	n.d.	n.d.	n.d.	n.d.	n.d.	n.d.	n.d.	n.d.	n.d.	n.d.	n.d.
Eu	n.d.	0.19	n.d.	n.d.	n.d.	n.d.	n.d.	n.d.	n.d.	n.d.	n.d.	n.d.	n.d.	n.d.	n.d.	n.d.	n.d.	n.d.
Tb	n.d.	0.2	n.d.	n.d.	n.d.	n.d.	n.d.	n.d.	n.d.	n.d.	n.d.	n.d.	n.d.	n.d.	n.d.	n.d.	n.d.	n.d.
Yb	n.d.	0.82	n.d.	n.d.	n.d.	n.d.	n.d.	n.d.	n.d.	n.d.	n.d.	n.d.	n.d.	n.d.	n.d.	n.d.	n.d.	n.d.
Lu	n.d.	0.12	n.d.	n.d.	n.d.	n.d.	n.d.	n.d.	n.d.	n.d.	n.d.	n.d.	n.d.	n.d.	n.d.	n.d.	n.d.	n.d.
Co	13	48	20	46	15	55	45	45	52	27	44	58	69	34	17	23	32	49
Hf	n.d.	0.4	n.d.	n.d.	n.d.	n.d.	n.d.	n.d.	n.d.	n.d.	n.d.	n.d.	n.d.	n.d.	n.d.	n.d.	n.d.	n.d.
Sc	n.d.	35.8	n.d.	3	n.d.	n.d.	18	10	13	14	27	9	1	n.d.	n.d.	13	n.d.	n.d.
U	1	n.d.	1	1	1	2	2	1	1	1	1	2	1	1	1	1	1	1
ε_{Nd}	n.d.	6.44	n.d.	n.d.	n.d.	n.d.	n.d.	n.d.	n.d.	n.d.	n.d.	n.d.	n.d.	n.d.	n.d.	n.d.	n.d.	n.d

Table 3. Whole rock chemical analyses from the Avdella mélange

Sample	P19	P24i	P25i	P41	P65
Chemical affinity	e-MORB	e-MORB	n-MORB	High-Ti MORB	e-MORB
Locality	D	G	H	L	V
Major elements by XRF (wt %)					
SiO_2	45.51	44.32	45.14	48.00	45.97
TiO_2	1.92	2.05	1.41	2.55	1.44
Al_2O_3	14.96	16.07	16.23	13.01	16.00
Fe_2O_{3T}	12.79	11.85	10.35	15.69	9.12
MnO	0.25	0.19	0.16	0.27	0.19
MgO	8.67	5.91	7.98	4.88	8.08
CaO	5.86	6.92	10.16	8.56	7.20
Na_2O	3.08	4.14	3.10	4.42	3.92
K_2O	0.34	1.44	0.38	0.24	0.28
P_2O_5	0.34	0.47	0.19	0.28	0.30
L.O.I	5.45	6.90	4.58	2.94	6.91
Total	99.17	100.26	99.68	100.84	99.41
Trace elements by XRF (ppm)					
Ba	58	280	53	b.d.	172
Rb	15	30	16	9	18
Sr	266	288	114	115	291
Y	27	32	28	45	24
Zr	144	182	95	127	95
Nb	22	58	13	14	29
Th	b.d.	5	b.d.	1	3
Pb	b.d.	1	5	b.d.	20
Ga	19	17	17	20	20
Zn	111	92	75	99	84
Cu	44	38	86	57	57
Ni	265	23	184	30	52
V	169	223	198	380	314
Cr	195	21	315	38	127
Trace elements by INAA (ppm)					
La	26	55	10	12.7	28
Ce	74	74	39	30	n.d.
Nd	37	29	34	19	24
Sm	n.d.	n.d.	n.d.	5.29	n.d.
Eu	n.d.	n.d.	n.d.	1.78	n.d.
Tb	n.d.	n.d.	n.d.	1	n.d.
Yb	n.d.	n.d.	n.d.	4.43	n.d.
Lu	n.d.	n.d.	n.d.	0.66	n.d.
Co	75	56	51	42.8	37
Hf	n.d.	n.d.	n.d.	3.8	n.d.
Sc	33	22	29	35.3	14
Ta	n.d.	n.d.	n.d.	1	n.d.
Th	n.d.	n.d.	n.d.	1.5	n.d.
U	2	3	2	0.6	2
ε_{Nd}	n.d.	n.d.	n.d.	5.21	n.d.

the lavas and dykes (Fig. 3a) cover all the geochemical spectrum of magma types that have been described by other authors (e.g. D. Kostopoulos, unpub. Ph.D. thesis, Univ. Newcastle, 1989), namely MORB, transitional MORB/IAT, IAT and boninite. Following Capedri *et al*. (1996), we distinguish high-Cr and low-Cr boninitic rocks. Nomenclature of plutonic rocks is based on petrography, except for the distinction of diorite from gabbro on the basis of SiO_2 content ($> 52\%$ SiO_2). Within the Avdella mélange (Table 3), three types of MORB are recognized. Normal (n-MORB) and enriched (e-MORB) relatively unfractionated basalts are distinguished on the basis of abundance of high-field strength elements such as Zr and Nb. High-Ti MORB is more fractionated, with low Mg number and high TiO_2.

4.b. Alteration

The rocks of the Aspropotamos Complex have experienced sea-floor upper zeolite to greenschist-facies hydrothermal alteration, with amphibolite-facies metamorphism of the Loumnitsa Complex. Samples were selected in the field as not showing strong hydrothermal alteration. Using loss on ignition (LOI) values as a further measure of the degree of alteration, only five out of the original 40 analytical samples were rejected because they showed LOI $> 4.5\%$, which Capedri *et al*. (1996) used as an upper limit for further geochemical consideration.

Valsami-Jones & Cann (1994) studied hydrothermally altered rocks of the Eastern Aspropotamos Complex. They showed that most of the lavas and dykes were located in the regional recharge zone and showed little alteration. They studied in detail localized discharge zones, characterized by the presence of epidosites and stockworks, in lavas of transitional IAT/boninite and boninite geochemistry. They found evidence for mobility of REE and $^{143}Nd/^{144}Nd$ compositions only in the epidosites and stockworks, but concluded from $^{87}Sr/^{86}Sr$ determinations that in both the regional recharge zone and the discharge

Table 4. Sm–Nd isotope determinations from the Pindos Ophiolite and Avdella mélange

Sample	Texture	Rock type	Sm ppm	Nd ppm	$^{147}Sm/^{144}Nd$	$^{143}Nd/^{144}Nd$	ε_{Nd}
Pindos Ophiolite							
P3	Porphyritic	Boninite lava	0.33	0.91	0.2160	0.51271	1.0
P5	Holocrystalline	IAT/MORB gabbro	0.53	1.33	0.2394	0.51301	6.4
P6	Porphyritic	Boninite lava	0.53	1.48	0.2147	0.51273	1.4
P15	Aphyric	IAT lava	1.73	4.39	0.2388	0.51304	7.0
P61i	Aphyric	IAT dyke	1.61	3.61	0.2703	0.51310	7.5
P63	Porphyritic	Boninite dyke	0.34	0.95	0.2147	0.51269	0.6
P64	Aphyric	Boninite dyke	0.67	1.77	0.2302	0.51283	3.0
Avdella Mélange							
P41	Amygdaloidal	High-Ti MORB lava	6.29	22.19	0.1715	0.51288	5.4

For ε_{Nd} determinations, constants used are: $^{143}Nd/^{144}Nd = 0.512638$ and $^{147}Sm/^{144}Nd = 0.1967$. Age assumed to be 165 Ma for Pindos Ophiolite and 210 Ma for Avdella Mélange.

https://doi.org/10.1017/S0016756804009215 Published online by Cambridge University Press

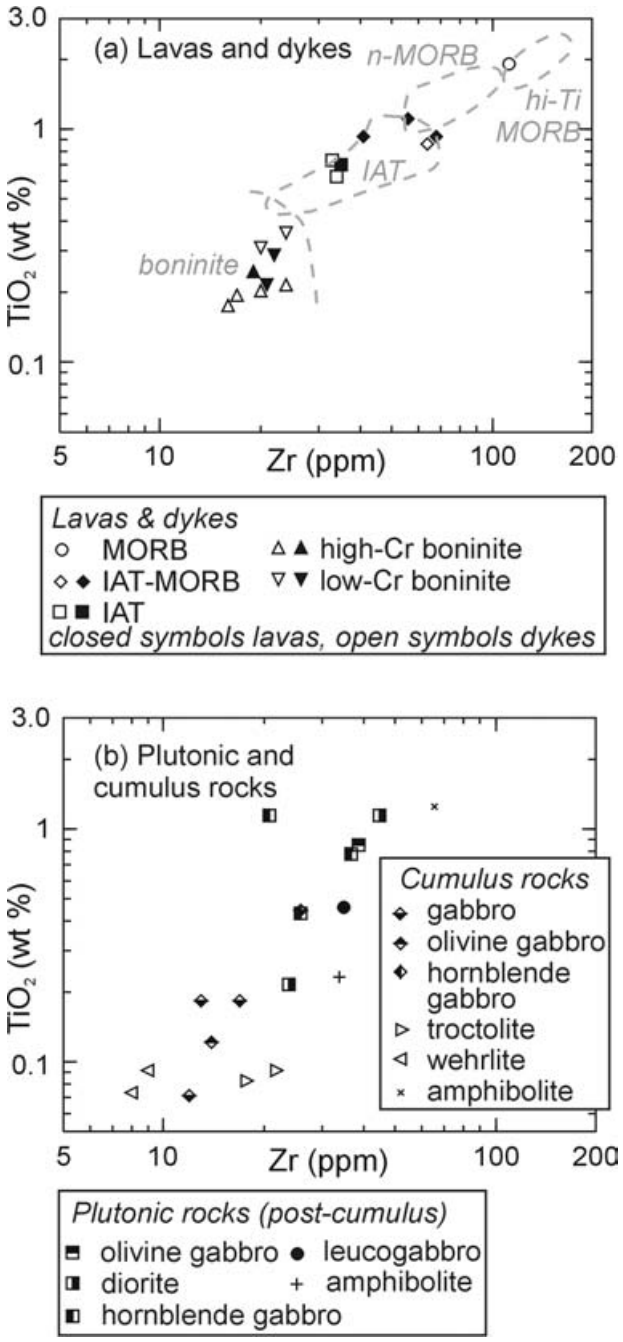

Figure 3. Variation of TiO_2 with Zr for the analysed samples from the Pindos Ophiolite Complex: (a) lavas and dykes; fields based on nomenclature of Capedri *et al*. (1980), Dupuy *et al*. (1984), and Jones, Robertson & Cann (1991) for the Pindos Ophiolite Complex; (b) plutonic and cumulus rocks.

epidosites, Sr composition was about half-way between likely protolith composition and the composition of Jurassic sea-water. Other LILE probably show similar degrees of mobility in the hydrothermally altered rocks. They concluded that in the discharge zones there was a small shift towards lower $^{143}Nd/^{144}Nd$ values with increasing alteration. However, 37% of their sample pairs show an increase in $^{143}Nd/^{144}Nd$ values in the more altered rock and 75% show variation within cited analytical error. Thus the observed differences are not statistically significant and we interpret their data to mean that Nd (together with other REE) is essentially immobile, particularly away from the highly altered epidosites.

Plots of mantle-normalized incompatible elements (Fig. 5) provide an indication of which elements show scatter and are therefore likely influenced by hydrothermal alteration. Of elements well above the detection limit, Sr and K, both abundant in sea-water, show the greatest scatter in boninites, with Ba and Th also showing some scatter. Valsami-Jones & Ragnarsdóttir (1997) showed that both Th and U are mobile in the hydrothermal systems of the Pindos Ophiolite. Elements such as Ba, Rb and K all show no systematic variation with Sr, except that samples with low Sr generally have low K.

4.c. Major and trace element geochemistry of lavas and dyke rocks

Major element variation (Figs 2, 4) is similar to that reported by other authors and will not be discussed in detail here. Using FeO_T/MgO as an index of fractionation, boninite, IAT and MORB compositions show different linear trends of increasing TiO_2 with increasing fractionation both from the literature (Pe-Piper & Piper, 2002, fig. 72c) and for the new analyses (Fig. 4a). MORB rocks from the Pindos Ophiolite (reported by others and in this paper) have FeO_T values of 8.5–10 at MgO = 8.0, within the range of normal MORB and showing no evidence of elevated potential temperature in the mantle (cf. Lassiter & dePaolo, 1997).

Rare earth elements (Fig. 5d) show similar abundances to those previously reported from the Pindos Ophiolite (Dupuy *et al*. 1984) with a progressive decrease in abundance in REE from MORB through IAT to boninite. Chondrite-normalized REE patterns are flat for MORB and transitional MORB/IAT; they show moderately negative fractionation from light to heavy REE for IAT, and a typical convex-downward profile for boninite. Most dyke rocks (open symbols in Fig. 5d) show a very small negative Eu anomaly compared to corresponding lavas. High-Cr and low-Cr boninites show essentially identical REE patterns, except for sample P64 which shows relatively more elevated middle and heavy REE.

When normalized to primitive mantle (Fig. 5), the REE and high-field strength elements (HFSE) show relatively flat patterns for MORB and a progressive slight increase in more incompatible elements (from Ce to Y) in IAT rocks (Fig. 5a). Rb and Ba are consistently about 20 × primitive mantle for both rock types. Sr and K appear enriched by hydrothermal processes. For the boninite samples (Fig. 5b), Rb is very consistent at 25–30 × primitive mantle, but other

https://doi.org/10.1017/S0016756804009215 Published online by Cambridge University Press

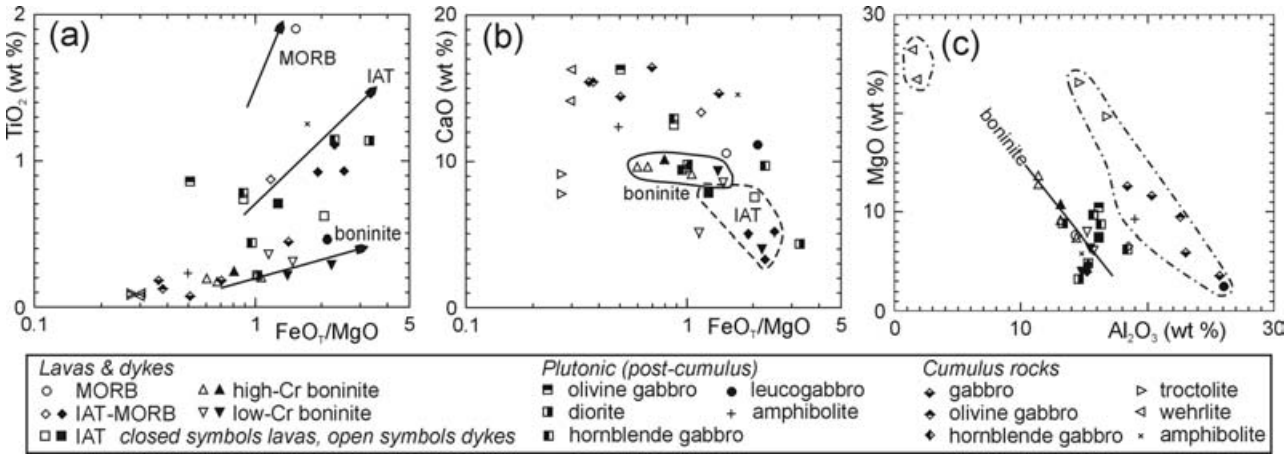

Figure 4. Variation of selected major elements for the analysed samples from the Pindos Ophiolite Complex. (a) TiO_2 v. FeO_T/MgO (arrows show trends for MORB, IAT and boninite based on Bébien *et al*. 1980, as modified by Pe-Piper & Piper, 2002); (b) CaO v. FeO_T/MgO (showing fields for boninite and IAT lavas and dykes); (c) MgO v. Al_2O_3 (showing trend for boninite lavas and dykes and fields for cumulus rocks).

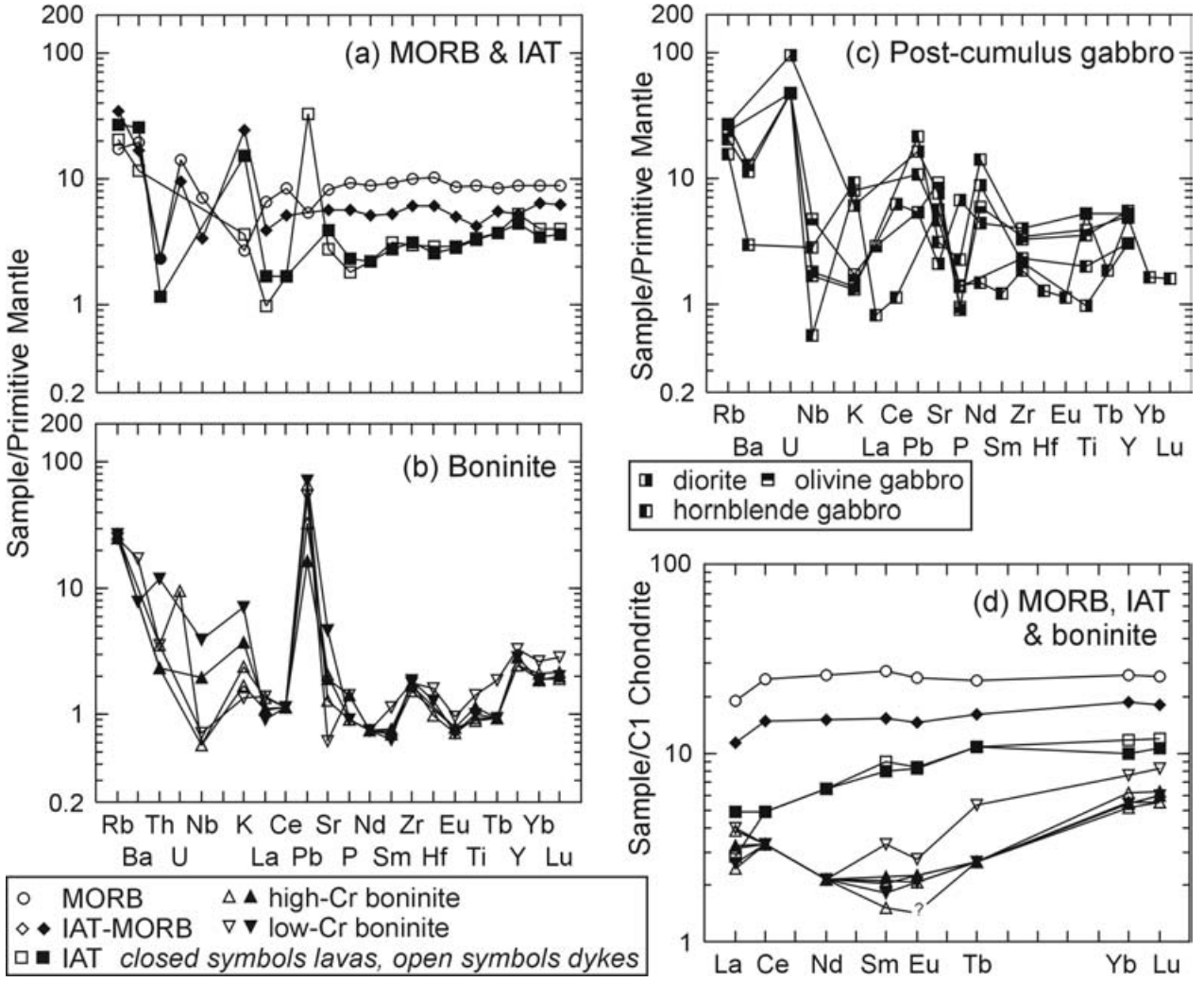

Figure 5. Plots of selected incompatible trace elements normalized to primitive mantle for (a) MORB and IAT dykes and lavas; (b) boninite dykes and lavas; (c) magmatic plutonic (post-cumulus) rocks; (d) REE normalized to chondrite for MORB, IAT and boninite dykes and lavas.

https://doi.org/10.1017/S0016756804009215 Published online by Cambridge University Press

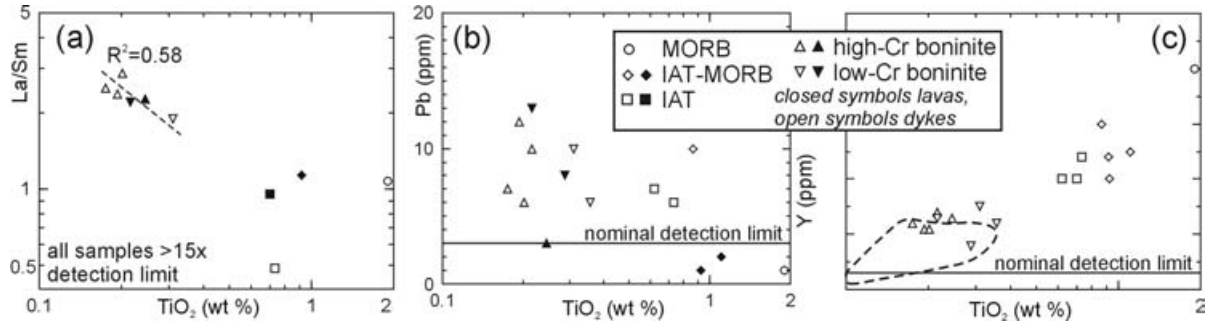

Figure 6. Variation of some elements with TiO_2 for the lavas and dykes of the Pindos Ophiolite Complex. (a) La/Sm (analyses by INAA only); (b) Pb; (c) Y, also showing corresponding field for Argolis boninites (dashed line), excluding outliers (data of Dostal *et al*. 1991 and Capedri *et al*. 1996).

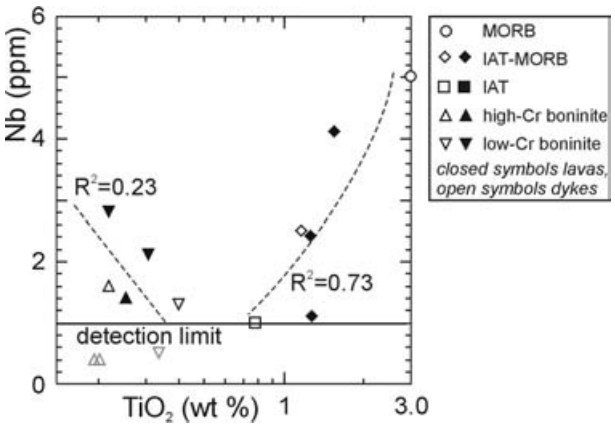

Figure 7. Plot of Nb v. TiO_2 for all Pindos lavas and dykes.

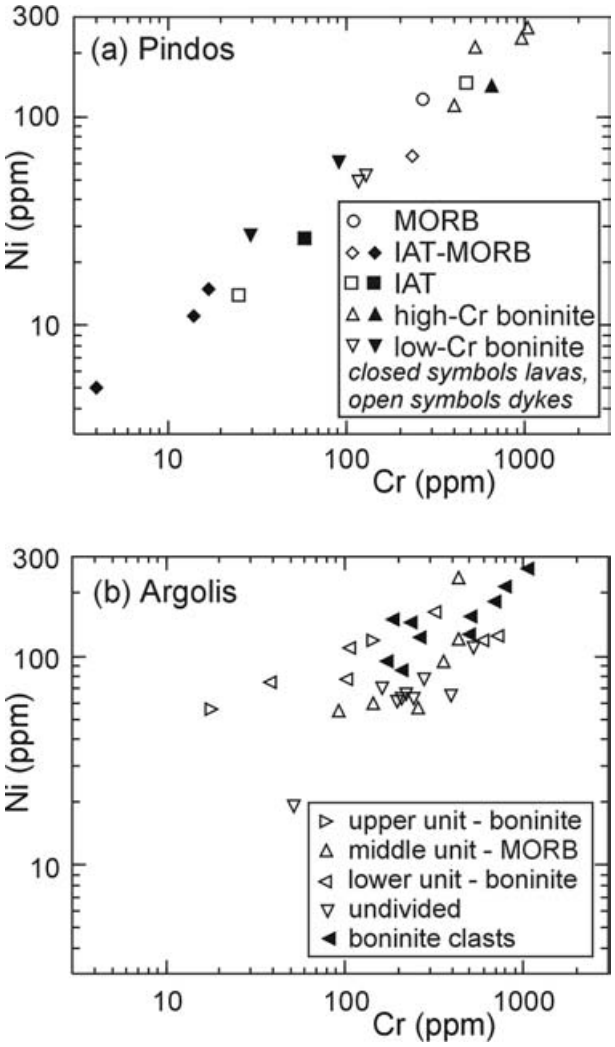

Figure 8. Variation of Ni and Cr content by rock type for lavas and dykes (a) for Pindos Ophiolite Complex and (b) for the Argolis Ophiolite (data of Dostal *et al*. 1991 and Capedri *et al*. 1996).

LILE are highly variable, with values below detection limits in several samples. Pb is progressively enriched in rocks with decreasing TiO_2 content (Fig. 6b) and is strongly enriched in boninite (Fig. 5b). The REE show consistent behaviour (except P64, noted above), but Sr is highly variable. Variability in P is related to analytical precision at low concentrations. Other HFSE are quite consistent, with positive anomalies of Zr and Hf. The elements Hf, Zr, V and Y (Fig. 6c) all decrease systematically with decreasing TiO_2 content of the lavas and dykes, whereas a systematic increase is shown by Pb (Fig. 6b) and La/Sm (Fig. 6a). Nb appears to decrease progressively from MORB to IAT and then increase in the boninites (Fig. 7), although given analytical uncertainties close to the detection limit these trends must be treated with caution.

The boninites can be divided into high-Cr and low-Cr types on the basis of their Cr and Ni content (Fig. 8), with a gap in Cr abundances between 100 and 300 ppm. The ratio of Cr to Ni (3:1) is almost constant over a wide range of compositions. Petrographically, the only consistent difference between the high-Cr and low-Cr types is that the high-Cr types are strongly phenocrystic, whereas the low-Cr types have sparse or no phenocrysts.

4.d. Sm/Nd isotopes

Sm/Nd isotope compositions (Table 4) expressed as ε_{Nd} show no evidence for hydrothermal alteration, since ε_{Nd} shows a linear relationship with $^{147}Sm/^{144}Nd$

https://doi.org/10.1017/S0016756804009215 Published online by Cambridge University Press

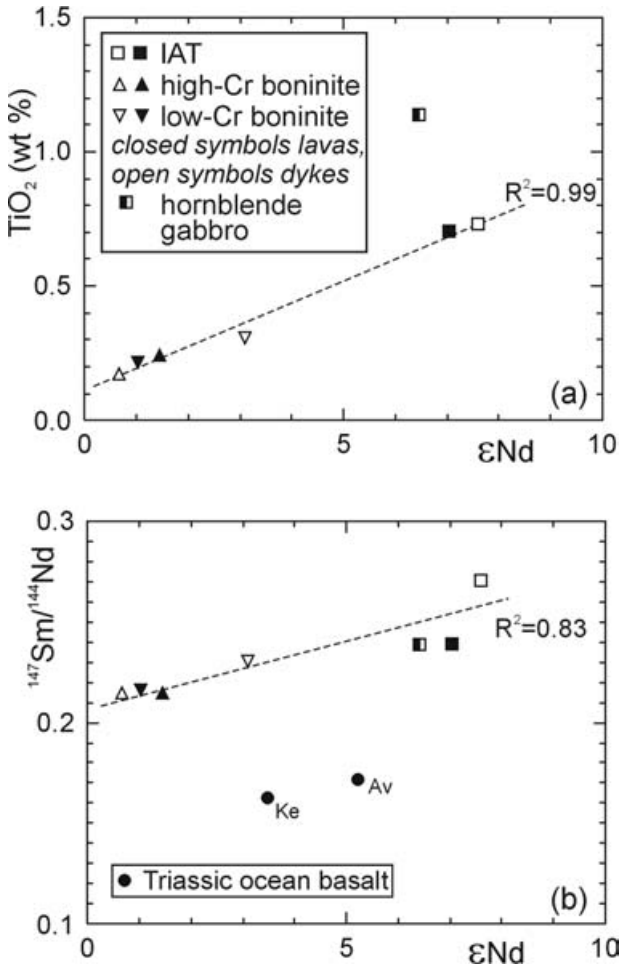

Figure 9. Plots showing variation in ε_{Nd} for Pindos Ophiolite rocks, dashed lines show linear regression for lavas and dykes only. (a) Variation with TiO_2; (b) variation with $^{147}Sm/^{144}Nd$. Also shown are Triassic samples from Avdella mélange (Av – high-Ti MORB: this paper) and Kerassies (Ke – MORB: Pe-Piper, 1998).

(Fig. 9b). The single determination on a magmatic plutonic rock (P5) also falls on this trend. Values of ε_{Nd} range from 7.6–7.0 for IAT lava and dyke rocks, 6.4 for IAT/MORB gabbro (Richard & Allègre, 1980, reported 8.0 for a Pindos MORB gabbro), to 3.1–0.7 for boninitic rocks (Valsami-Jones & Cann, 1994, reported ε_{Nd} of 2.4 and 4.3). When plotted against TiO_2, ε_{Nd} for all the lavas and dykes show a straight line trend, with only the plutonic rock falling off the trend (Fig. 9a). A similar linear trend is shown by the La/Sm ratio.

4.e. Plutonic rocks

The cumulus rocks show low contents of TiO_2 (0.07–0.18%, with the exception of 0.43% in P11ii), Zr (12–26 ppm), Y (1–8 ppm) and V (30–173 ppm), with the troctolites having the most mafic compositions (Table 2). In contrast, the post-cumulus (magmatic) gabbros and diorites are richer in these elements containing 0.21–1.11% TiO_2, 21–45 ppm Zr, 5–25 ppm Y and 184–230 ppm V (with one exception, sample P5, with 872 ppm V). The cumulus rocks are quite different from more evolved post-cumulus plutonic rocks in their high Al_2O_3 contents (Fig. 4c). Variations of MgO, Ni and Cr with FeO_T/MgO (Fig. 10) are compatible with olivine fractionation that was more extensive in the post-cumulus plutonic rocks. The CaO variation shows scatter in the cumulus rocks and a linear trend in the post-cumulus rocks, indicating that plagioclase and/or clinopyroxene fractionation occurred only in the latter (Fig. 4b). The contents of TiO_2 (Fig. 4a), Zr (Fig. 3b) and Cr (Fig. 10b) in the post-cumulus gabbros and diorites are in the range of IAT and boninite. Post-cumulus rocks show a linear correlation of TiO_2 with Zr, indicating incompatible behaviour during fractionation (Fig. 3b). The trend is

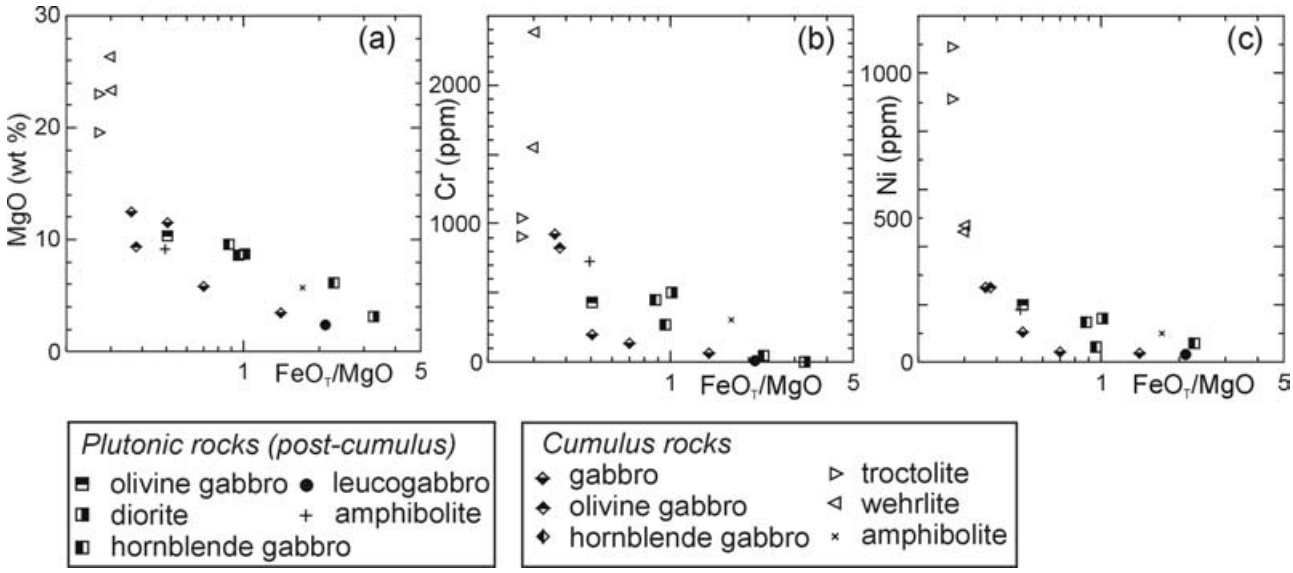

Figure 10. Plots showing variation with FeO_T/MgO of (a) MgO, (b) Cr and (c) Ni for plutonic and cumulus rocks of the Pindos Ophiolite Complex.

https://doi.org/10.1017/S0016756804009215 Published online by Cambridge University Press

the same as for the lavas and dykes, but the range is a little lower, with several of the post-cumulus rocks having low Zr and TiO_2 contents in the same range as the boninite dykes.

4.f. Avdella mélange

Our analyses of Triassic volcanic rocks of the Avdella mélange (Table 3) confirm previous work by Jones & Robertson (1991) in identifying compositions of both n-MORB and of e-MORB (WPB/MORB of Jones & Robertson), interpreted as representing seamount volcanism. The only isotope determination is from a high-Ti MORB rock with REE and Nb abundances suggesting a n-MORB parent. It has a relatively low ε_{Nd} of 5.2.

5. Discussion

5.a. Geochemical characteristics of the Pindos boninites

Several common geochemical features of fore-arc boninites are recognized in the Pindos boninites. These include high Mg and Si, relative depletion in the middle REE, low concentrations of elements such as Nb and Ti, relatively high Hf contents, and typically $Zr_N/Hf_N > 1$. There is a general consensus that such features result from low-pressure melting of residual harzburgite from which basaltic magma had already been extracted (Crawford, Falloon & Green, 1989; Falloon & Danyushevsky, 2000). Enrichment of LILE relative to HFSE has been generally intepreted as resulting from transport by hydrous fluids derived from the subducting slab (e.g. Stern *et al*. 1991). The behaviour of HFSE has been commonly ascribed to an OIB component (e.g. Kostopoulos & Murton, 1992; Wendt *et al*. 1997).

The origin of high Zr and Hf compared with Ti and the middle REE in boninites is a contentious issue. It has been ascribed either to OIB magma sources (e.g. Falloon & Crawford, 1991; Stern *et al*. 1991) or to partial melting of mafic source material in the amphibolite stability field. This mafic source may be either in the subducted slab (Taylor *et al*. 1994) or from mafic veins within the mantle wedge (Pearce *et al*. 1999). We have no new data to contribute to the question of why high Zr and Hf occur.

Pb contents are higher in most Pindos boninites than in IAT and are even lower in IAT/MORB. Pb is generally associated with terrigenous sediment. Rb shows a narrow range of compositions for all rock types and is as enriched as Pb in the boninites (Fig. 5). All of the other LILE show a large amount of scatter.

High-Cr and low-Cr boninites differ principally in phenocryst abundance. A similar relationship was noted in Argolis, where the high Cr boninites are strongly porphyritic rocks that include chrome spinel (Capedri *et al*. 1996). Chrome spinel was not conclusively identified in the Pindos boninites, which show much less scatter in Ni:Cr ratio than do the Argolis boninites (Fig. 8), suggesting that the high Cr resides in a single mineral phase, probably clinopyroxene.

5.b. Plutonic rocks of the Pindos Ophiolite

The post-cumulus gabbros and diorites have Ti and Zr contents (Fig. 3) and other HFSE abundances (Fig. 5) that resemble IAT and boninite lavas and dykes. In contrast, in the cumulus rocks, the TiO_2 contents of 0.07–0.2% (Fig. 3b), high Cr (Fig. 10b), the early crystallization of plagioclase and the paucity of orthopyroxene (Appendix) are all features that Bébien *et al*. (1998) identified as characteristic of MORB-related cumulus rocks. It thus appears that the IAT and boninitic magmas intruded a pre-existing cumulus sequence. This is similar to analogous rocks occurring in the eastern-type Albanian ophiolites, which form the northward continuation of the Pindos Ophiolite (Hoeck *et al*. 2002). The cumulus sequences of these ophiolites generally contain wehrlite, troctolite and gabbro, which have been intruded by Ti-poor IAT and boninitic magmas (Bébien *et al*. 1998, 2000; Robertson & Shallo, 2000).

5.c. The origin of low Nd: subducted sediment or mantle plume?

Studies of the isotopic composition of modern boninites (Hickey & Frey, 1982; Cameron, McCulloch & Walker, 1983) and ancient boninites from various locations show that they have ε_{Nd} of 0 to +7 compared with > +7 for MORB and intermediate values for IAT. Pindos IAT magmas, presumably sourced in the mantle wedge of the supra-subduction ophiolite, have ε_{Nd} of about +7, not unreasonable for depleted oceanic asthenosphere. To account for the low ε_{Nd} of the boninites requires an additional source of Sm and Nd with low ε_{Nd}. In the boninite samples, the correlation of certain elements with either TiO_2 or ε_{Nd} (Figs 6, 7, 9) is interpreted to mean that as the depleted harzburgite source became increasingly refractory, then small quantities of elements from other sources became an increasingly important component of the melt. The elements contributed from this source would include the REE, as seen by variation in La/Sm (Fig. 6a) and Sm–Nd isotopes (Fig. 9a), Pb (Fig. 6b) and possibly Nb (Fig. 7). Probable candidates for such contributions are subducted terrigenous sediments or OIB-type mantle.

The nature of sediment subducted during the development of the Pindos Ophiolite is recorded in the Avdella mélange and includes terrigenous turbidites sourced in the Hercynian granites and metamorphic rocks of the Pelagonian zone (Jones & Robertson, 1991). Sm/Nd isotopes from Hercynian granitoid rocks of Thessaly (Pe-Piper, 1998) have an initial ε_{Nd} of −5

https://doi.org/10.1017/S0016756804009215 Published online by Cambridge University Press

to −7 at 300 Ma, corresponding to $\varepsilon_{Nd} = -7$ to −8 at 150 Ma. Thus, a relatively small proportion of Sm and Nd derived from subducted terrigenous turbidites sourced by such Hercynian terranes could account for the low ε_{Nd} in the Pindos boninites. Boninites are enriched in Pb, which is abundant in subducted terrigenous sediment and is readily transported by aqueous fluids (Keppler, 1996). However, Nd and Sm would require transport by a silicate melt, rather than by aqueous fluids, and many geochemical features of the boninites are quite inconsistent with a source influenced by aqueous fluids or even melts derived from subducted sediment. The REE and HFSE are not readily transported in aqueous fluids. Nb is characteristically in low abundance in terrigenous sediment, yet is higher than in some IAT/MORB in some boninites (Fig. 7) and shows no systematic behaviour with Cr content. Projection of the linear trend between TiO_2 and ε_{Nd} (Fig. 9a) to zero TiO_2 corresponds to ε_{Nd} of only −1.5, quite different from subducted sediment. We therefore interpret the REE and HFSE signature of the boninites as derived from minor OIB-type source within the mantle wedge. Similar interpretations have been made for the Troodos Ophiolite (Kostopoulos & Murton, 1992) and the voluminous boninitic magmas of the southwest Pacific (Wendt *et al*. 1997; Pearce *et al*. 1999).

5.d. Regional evidence for an OIB source

A Triassic mantle plume has been inferred previously from studies of Triassic rift-related rocks, based on radiogenic isotopes (Pe-Piper, 1998) and Nb enrichment (Dixon & Robertson, 1999). Enriched MORB or alkaline basalt of inferred seamount origin is known from several ophiolitic mélanges, including Pagondas (Simantov & Bertrand, 1987), Helikon (Aslanidis, 1993) and Avdella. All of these observations suggest that OIB magma would likely be a common feature of oceanic mantle within the Pindos Ocean.

We have attempted to detect any regional variations in the abundance of this OIB component. Based on the relationship in Figure 7 and the high Nb reported by Dixon & Robertson (1999), we have compared the Nb/Ti ratio for boninites and for unfractionated MORB from various western Greek localities. The most recent comprehensive geochemical data set is for Argolis (Dostal *et al*. 1991; Capedri *et al*. 1996), 300 km along strike, but we have also used data from other ophiolites summarized by Pe-Piper & Piper (2002). No systematic variation in Nb/Ti ratio, or other HFSE abundances or ratios, was detected.

6. Conclusions

The boninites of the Pindos Ophiolite geochemically resemble classical boninites. They were derived from partial melting of depleted harzburgite containing some OIB-type mantle. This OIB source contributed most of the REE and Nb (and probably Zr and Hf) in the boninites, resulting in low ε_{Nd}. High Pb, Rb and other LILE were probably derived by aqueous transport from the subducting slab. The OIB components in the mantle are consistent with the widespread evidence for mantle plumes during Triassic rifting of the northern Gondwanan margin.

Acknowledgements. This work was supported by a Natural Sciences and Engineering Research Council of Canada Discovery Grant to GPP. We thank D. J. W. Piper and the journal referees for their thorough reviews which resulted in substantial improvements to this paper.

References

ASLANIDIS, P. 1993. Geological and geochemical criteria on the classification of Mesozoic volcanites in the Helikon Mountains, Greece. *Bulletin of the Geological Society of Greece* **28**, 123–37.

BÉBIEN, J., OHNENSTETTER, D., OHNENSTETTER, M. & VERGELY, P. 1980. Diversity of Greek ophiolites: birth of oceanic basins in transcurrent systems. *Ofioliti* **2**, 129–97.

BÉBIEN, J., SHALLO, M., MANIKA, K. & GEGA, D. 1998. The Shebenik massif (Albania): a link between MOR and SSZ-type ophiolites? *Ofioliti* **23**, 7–15.

BÉBIEN, J., DIMO-LAHITTE, A., VERGELI, D., INSERGUEIX-FILIPPI, P. & DUPEYRAT, L. 2000. Albanian ophiolites: I. magmatic and metamorphic processes associated with the initiation of a subduction. *Ofioliti* **25**, 39–45.

CAMERON, W. E., MCCULLOCH, M. T. & WALKER, D. A. 1983. Boninite petrogenesis: chemical and Nd-Sr isotopic constraints. *Earth and Planetary Science Letters* **65**, 75–89.

CAPEDRI, S., GARUTI, G. & ROSSI, A. 1978. Rodingites from Pindos. Constraints on the 'rodingite problem'. *Neues Jahrbuch für Mineralogie, Abhandlungen* **132**, 242–63.

CAPEDRI, S., GRANDI, R., PHOTIADES, A. & TOSCANI, L. 1996. 'Boninitic' clasts from the Mesozoic olistostromes and turbidites of Angelokastron (Argolis, Greece). *Geological Journal* **31**, 301–22.

CAPEDRI, S., VENTURELLI, G., BÉBIEN, J. & TOSCANI, L. 1981. Low and high Ti ophiolites in northern Pindos: petrological and geological constraints. *Bulletin Vulcanologique* **44**, 439–49.

CAPEDRI, S., VENTURELLI, G., BOCCHI, G., DOSTAL, J., GARUTI, G. & ROSSI, A. 1980. The geochemistry and petrogenesis of an ophiolitic sequence from Pindos, Greece. *Contributions to Mineralogy and Petrology* **74**, 189–200.

CAPEDRI, S., VENTURELLI, G. & TOSCANI, L. 1982. Petrology of an ophiolitic cumulate sequence from Pindos, Greece. *Geological Journal* **17**, 223–42.

CRAWFORD, A. J., FALLOON, T. J. & GREEN, D. H. 1989. Classification, petrogenesis and tectonic setting of boninites. In *Boninites and related rocks* (ed. A. J. Crawford), pp. 1–49. London: Unwin Hyman.

DIXON, J. E. & ROBERTSON, A. H. F. 1999. Are multiple plumes implicated in the Triassic break-up of the Gondwanan margin in the eastern Mediterranean region. *Journal of Conference Abstracts* **4**(1), 314.

DOSTAL, J., TOSCANI, L., PHOTIADES, A. & CAPEDRI, S. 1991. Geochemistry and petrogenesis of Tethyan

ophiolites from northern Argolis (Peloponnesus, Greece). *European Journal of Mineralogy* **3**, 105–21.

DUPUY, C., DOSTAL, J., CAPEDRI, S. & VENTURELLI, G. 1984. Geochemistry and petrogenesis of ophiolites from Northern Pindos (Greece). *Bulletin Volcanologique* **47**, 39–46.

FALLOON, T. J. & CRAWFORD, A. J. 1991. The petrogenesis of high-calcium boninite lavas dredged from the northern Tonga ridge. *Earth and Planetary Science Letters* **102**, 375–94.

FALLOON, T. J. & DANYUSHEVSKY, L. V. 2000. Melting of refractory mantle at 1.5, 2 and 2.5 GPa under anhydrous and H_2O-undersaturated conditions: implications for the petrogenesis of high-Ca boninites and the influence of subduction components on mantle melting. *Journal of Petrology* **41**, 257–83.

HICKEY, R. & FREY, F. A. 1982. Geochemical characteristics of boninite series volcanics: implications for their source. *Geochimica et Cosmochimica Acta* **46**, 2099–2115.

HOECK, V., KOLLER, F., MEISEL, T., ONUZI, K. & KNERINGER, E. 2002. The Jurassic Albanian ophiolites: MOR- vs. SSZ-type ophiolites. *Lithos* **65**, 143–64.

JONES, G. & ROBERTSON, A. H. F. 1991. Tectono-stratigraphy and evolution of the Mesozoic Pindos ophiolite and related units, northwestern Greece. *Journal of the Geological Society, London* **148**, 267–88.

JONES, G., ROBERTSON, A. H. F. & CANN, J. R. 1991. Genesis and emplacement of the supra-subduction zone Pindos Ophiolite, northwestern Greece. In *Ophiolite Genesis and Evolution of the Oceanic Lithosphere* (ed. Tj. Peters *et al*.), pp. 771–99. Ministry of Petroleum and Minerals, Sultanate of Oman.

KEPPLER, H. 1996. Constraints from partitioning experiments on the composition of subduction-zone fluids. *Nature* **380**, 237–40.

KOSTOPOULOS, D. & MURTON, B. J. 1992. Origin and distribution of components in boninite genesis: significance of the OIB component. In *Ophiolites and their modern oceanic analogues* (eds L. M. Parson, B. J. Murton and P. Browning), pp. 133–54. Geological Society of London, Special Publication no. 60.

LASSITER, J. C. & DEPAOLO, D. J. 1997. Plume/lithosphere interaction in the generation of continental and oceanic flood basalts: chemical and isotopic constraints. *Geophysical Monograph* **100**, 335–55.

PEARCE, J. A., KEMPTON, P. D., NOWELL, G. M. & NOBLE, S. R. 1999. Hf-Nd element and isotope perspective on the nature of mantle and subduction components in western Pacific arc-basin systems. *Journal of Petrology* **40**, 1579–611.

PEARCE, J. A., LIPPARD, S. J. & ROBERTS, S. 1984. Characteristics and tectonic significance of supra-subduction zone ophiolites. In *Marginal Basin Geology* (eds B. P. Kokelaar and M. F. Howells), pp. 77–94. Geological Society of London, Special Publication no. 16.

PE-PIPER, G. 1998. The nature of Triassic extension-related magmatism in Greece: evidence from Nd and Pb isotope geochemistry. *Geological Magazine* **135**, 331–48.

PE-PIPER, G. & PIPER, D. J. W. 2002. *The Igneous Rocks of Greece*. Stuttgart: Borntraeger, 645 pp.

RASSIOS, A. 1991. Internal structure and pseudostratigraphy of the Dramala peridotite massif, Pindos Mountains, Greece. *Bulletin of the Geological Society of Greece* **25**, 293–305.

RASSIOS, A. & SMITH, A. G. 2000. Constraints on the formation and emplacement age of western Greece ophiolites (Vourinos, Pindos and Othris) inferred from deformation structures in peridotites. In *Ophiolites and ocean crust: new insights from field studies and the Ocean Drilling Program* (eds Y. Dilek, E. M. Moores, D. Elthon and A. Nicolas), pp. 473–83. Geological Society of America, Special Paper no. 349.

RICHARD, P. & ALLÈGRE, C. J. 1980. Neodymium and strontium isotope study of ophiolite and orogenic lherzolite petrogenesis. *Earth and Planetary Science Letters* **47**, 65–74.

ROBERTSON, A. H. F., CLIFT, P. D., DEGNAN, P. & JONES, G. 1991. Paleoceanography of the Eastern Mediterranean Neotethys. *Paleogeography, Paleoclimatology, Paleoecology* **87**, 289–343.

ROBERTSON, A. H. F. & SHALLO, M. 2000. Mesozoic–Tertiary tectonic evolution of Albania in its regional Eastern Mediterranean context. *Tectonophysics* **316**, 197–254.

ROGERS, N. W., MACLEOD, C. J. & MURTON, B. J. 1989. Petrogenesis of boninitic lavas from the Limassol Forest Complex, Cyprus. In *Boninites and related rocks* (ed. A. J. Crawford), pp. 288–313. London: Unwin Hyman.

SIMANTOV, J. & BERTRAND, J. 1987. Major and trace element goechemistry of the central Euboea basaltic rocks (Greece): possible geotectonic implications. *Ofioliti* **12**, 201–18.

SPRAY, J. G. & RODDICK, J. C. 1980. Petrology and $^{40}Ar/^{39}Ar$ geochronology of some Hellenic sub-ophiolite metamorphic rocks. *Contributions to Mineralogy and Petrology* **72**, 43–55.

STERN, R. J., MORRIS, J., BLOOMER, S. H. & HAWKINS, J. W. 1991. The source of the subduction component in convergent margin magmas: trace element and radiogenic evidence from Eocene boninites, Mariana forearc. *Geochimica et Cosmochimica Acta* **55**, 1467–81.

TAYLOR, R. N., NESBITT, R. W., VIDAL, P., HARMON, R. S., AUVRAY, B. & CROUDACE, I. W. 1994. Mineralogy, chemistry and genesis of the boninite series volcanics, Chichijima, Bonin Islands, Japan. *Journal of Petrology* **35**, 577–617.

VALSAMI-JONES, E. & CANN, J. R. 1994. Controls on the Sr and Nd isotopic compositions of hydrothermally altered rocks from the Pindos ophiolite, Greece. *Earth and Planetary Science Letters* **125**, 39–54.

VALSAMI-JONES, E. & RAGNARSDÓTTIR, K. V. 1997. Controls on uranium and thorium behaviour in ocean-floor hydrothermal systems: examples from the Pindos ophiolite, Greece. *Chemical Geology* **135**, 263–74.

WENDT, J. L., REGELOUS, M., COLLERSON, K. D. & EWART, A. 1997. Evidence for a contribution from two mantle plumes to island-arc lavas from northern Tonga. *Geology* **25**, 611–14.

WHITECHURCH, H. & PARROT, J. F. 1978. Ecailles métamorphiques infraperidotiques dans le Pinde septentrional (Grèce): croûte oceanique, métamorphisme et subduction. *Comptes Rendus de l'Academie des Sciences de Paris* **286**, 1491–4.

Appendix. Location, chemical affinity and petrography of the analysed samples

Sample	Petrographic affinity	Chemical affinity	Rock type	Locality (Fig. 1)	Petrographic notes
P6	Basalt	High-Cr boninite	Lava	A	Porphyritic with euhedral phenocrysts of orthopyroxene, clinopyroxene and plagioclase set in a groundmass of plagioclase microlites and devitrified glass. Many clinopyroxene crystals are optically zoned. Alteration minerals include chlorite, actinolite, quartz and dusty opaque minerals.
P14i	Basalt	IAT/MORB	Lava	B	Amygdaloidal (amygdales rare in P42). Fine-grained intersertal with tiny laths of plagioclase in a groundmass with devitrified glass and interstitial opaque minerals. In samples P24I and P42 branching plagioclase crystals (like spinifex texture) and smaller clinopyroxene crystals are developed. There are also amygdules filled with calcite, chlorite and quartz. Other alteration products include epidote and dusty opaques.
P39	Basalt	IAT/MORB	Lava	K	
P42	Basalt	IAT/MORB	Lava	M	
P15	Basalt	IAT	Lava	C	Altered intergranular, with plagioclase laths and smaller fibrous clinopyroxene crystals partially replaced by actinolite and chlorite. The groundmass in samples P25I, P59 is very fine-grained, containing a small proportion of devitrified glass and plagioclase microlites. The main alteration products are chlorite, albite, calcite, sericite, actinolite, quartz and Fe-Ti oxides that participate in high proportion in P59. P41 is amygdaloidal with chlorite filling the amygdules.
P59	Basalt	High-Ti MORB	Dyke	U	
P3	Basalt	Low-Cr boninite	Lava	A	Fine-grained, porphyritic with phenocrysts of clinopyroxene and albitized plagioclase in a groundmass of plagioclase and clinopyroxene microlites, with accessory opaque minerals. Many clinopyroxene phenocrysts are optically zoned and some have actinolite core. Other secondary minerals are albite, epidote, clinozoisite, chlorite, calcite and quartz. Devitrified glass is altered to chlorite.
P12i	Basalt	Low-Cr boninite	Lava	B	Medium-grained basalt with altered clinopyroxene crystals set in a microgranular groundmass. Alteration includes actinolite, epidote, dusty opaque minerals and clay minerals (the last in the groundmass). Opaque mineral grains are also present.
P64	Basalt	Low-Cr boninite	Dyke	U	Porphyritic with euhedral phenocrysts of clinopyroxene and plagioclase set in a groundmass of plagioclase microlites and devitrified glass. Many clinopyroxene crystals are optically zoned. Alteration minerals include chlorite, quartz and dusty opaque minerals.
P61i	Dolerite	IAT	Dyke	U	Medium-grained, granular. Highly altered with subhedral prismatic plagioclase and pseudomorphic actinolite after clinopyroxene. Other alteration products are chlorite, sericite, quartz, opaque minerals.
P2	Dolerite	Low-Cr boninite	Dyke	A	Medium-grained, intergranular, subophitic with anhedral clinopyroxene crystals between plagioclase laths. In samples P13, P53I all clinopyroxene crystals are replaced by actinolite. The main alteration products are chlorite, albite, actinolite, epidote, clinozoisite, calcite and quartz. P2 contains titanite and P13 opaque minerals.
P13	Dolerite	IAT	Dyke	B	
P45	Dolerite	n-MORB	Dyke	N	
P53i	Dolerite	High-Cr boninite	Dyke	R	
P63	Dolerite	High-Cr boninite	Dyke	U	
P58	Dolerite	High-Cr boninite	Dyke	U	Fine-grained, porphyritic with phenocrysts of clinopyroxene and albitized plagioclase set in a groundmass of plagioclase and clinopyroxene microlites. Many clinopyroxene phenocrysts are zoned, with actinolite in some cores. Other secondary minerals are albite, epidote, clinozoisite and quartz.
P22ii	Dolerite	High-Cr boninite	Dyke	F	Medium-grained, granular. Highly altered with subhedral prismatic plagioclases and pseudomorphic actinolite after clinopyroxene. Other alteration products are chlorite, sericite, quartz and opaque minerals.
P9	Leuco-gabbro	Low-Cr boninite	Magmatic	A	Granular, subophitic with subhedral prismatic plagioclase zoned crystals and anhedral clinopyroxene crystals (about 10%) filling the wedge-shaped spaces between plagioclases. Some clinopyroxene crystals are replaced by actinolite and chlorite. Other alteration minerals are albite, sericite, epidote and clinozoisite. Trace opaque minerals.
P22i	Diorite	High-Cr boninite	Magmatic	F	Medium-grained, subophitic with subhedral prismatic plagioclase and subhedral to anhedral interstitial clinopyroxene crystals. Some plagioclase crystals are replaced by albite and sericite; actinolite and chlorite develop in clinopyroxene pseudomorphs. Epidote and opaque minerals as alteration products occur in P46.
P46	Diorite	IAT/MORB	Magmatic	O	
P61ii	Hornblende gabbro	IAT/MORB	Magmatic	U	Medium-grained, granular with randomly oriented prismatic highly altered plagioclase crystals and secondary hornblende. Clinopyroxene crystals are pseudomorphically replaced by actinolite fibres. Other secondary minerals are albite, sericite, epidote and chlorite.
P5	Hornblende gabbro	Low-Cr boninite	Magmatic	A	Extreme orthocumulate texture. Plagioclase slightly altered to sericite and clay minerals. Postcumulus subhedral to euhedral hornblende occupies the interstices, altering to actinolite. Lesser amounts of clinopyroxene totally replaced by actinolite. Interstitial opaque minerals.
P10	Hornblende gabbro	High-Cr boninite	Magmatic	A	

https://doi.org/10.1017/S0016756804009215 Published online by Cambridge University Press

Appendix. Continued

Sample	Petrographic affinity	Chemical affinity	Rock type	Locality (Fig. 1)	Petrographic notes
P54i	Amphibolite	MORB	?Magmatic	S	Strongly tectonized with subhedral hornblende crystal orientation. Clinopyroxene crystals are totally replaced by actinolite. Sericite in prismatic plagioclase crystals. Interstitial opaque minerals are present.
P37	Olivine gabbro	IAT	Magmatic	J	Medium to fine grained, granular texture, inequigranular subhedral plagioclase, coarser subhedral to anhedral clinopyroxene and fine grained anhedral olivine. Rare opaque minerals. Fine-grained mylonitic zones penetrate the rock. Alteration is to actinolite, quartz, albite, serpentine and epidote.
P56	Gabbro (altered)		Cumulus	T	Medium grained subhedral plagioclase and subhedral to anhedral clinopyroxene as cumulus phases. Plagioclase is partially altered to epidote and minor albite, whereas the clinopyroxene is strongly altered (mostly pseudomorphs) to actinolite and minor chlorite.
P51	Gabbro		Cumulus	P	Coarse-grained with megacrysts of subhedral clinopyroxene (many are fractured) and partially altered plagioclase crystals. The main alteration minerals are albite, chlorite, actinolite, and sericite.
P4	Gabbro		Cumulus	A	Cumulus plagioclase and clinopyroxene. Some plagioclase crystals are altered to sericite and clay minerals. Some clinopyroxene crystals are altered to actinolite and chlorite. Some clinopyroxene crystals display exsolution lamellae of orthopyroxene. Rare opaque minerals as alteration products.
P11ii	Gabbro		Cumulus	A	Altered medium-grained, with cumulus texture. It is composed mainly of oriented cumulus plagioclase crystals, a few surrounded by single large crystals of postcumulus clinopyroxene, forming postcumulus texture. Alteration products include chlorite, epidote, clinozoisite, sericite, actinolite and chlorite. There are also fractures filled with prehnite, epidote and chlorite.
P52I	Olivine gabbro		Cumulus	Q	Medium-grained, inequigranular with subhedral prismatic plagioclase and anhedral clinopyroxene and olivine crystals. Some clinopyroxenes show tectonic fabrics with concave rims surrounded by small clinopyroxene and olivine neoblasts. Alteration products include sericite, actinolite, serpentine, clinozoisite and dusty opaque minerals.
P31	Troctolite		Cumulus	I	Medium-grained, granular with stout subhedral prismatic plagioclase, anhedral clinopyroxene and interstitial olivine crystals. In P31, there are small anhedral brown spinel crystals.
P32	Troctolite		Cumulus	I	
P50	Wehrlite		Cumulus	P	Medium-grained, granular with stout subhedral prismatic plagioclase, anhedral clinopyroxene and interstitial olivine crystals. Clinopyroxene crystals are altered to actinolite, olivine is altered to serpentine.
P49	Wehrlite		Cumulus	P	Coarse-grained, with equigranular subhedral clinopyroxene, anhedral olivine and a small proportion of orthopyroxene crystals. Some clinopyroxenes contain finer olivine inclusions. Olivine is partially altered.

https://doi.org/10.1017/S0016756804009215 Published online by Cambridge University Press